Carbon monoxide adsorption at forsterite surfaces as models of interstellar dust grains: An unexpected bathochromic (red) shift of the CO stretching frequency

(Article begins on next page)

20 April 2024

CARBON MONOXIDE ADSORPTION AT FORSTERITE SURFACES AS MODELS OF INTERSTELLAR DUST GRAINS: AN UNEXPECTED BATHOCHROMIC (RED) SHIFT OF THE CO STRETCHING FREQUENCY

Lorenzo Zamirri,[1,2] Stefano Pantaleone,[3] and Piero Ugliengo.[1,2,*]

[1]*Dipartimento di Chimica, Università degli Studi di Torino, via P. Giuria 7, I-10125, Torino, Italy.*
[2]*Nanostructured Interfaces and Surfaces (NIS) Centre, Università degli Studi di Torino, via P. Giuria 7, I-10125, Torino, Italy.*
[3]*Departament de Química, Universitat Autònoma de Barcelona, E-08193 Bellaterra, Spain.*

Abstract

Carbon monoxide (CO) is one of the most abundant species in the interstellar medium (ISM). In the colder regions of the ISM, it can directly adsorb onto exposed Mg cations of forsterite (Fo, Mg_2SiO_4), one of the main constituents of the dust grains. Its energetic of adsorption can strongly influence the chemico-physical evolution of cold interstellar clouds, thus a detailed description of this process is desirable. We recently simulated the CO adsorption on crystalline Fo surfaces by computer *ab initio* methods and, surprisingly, reported cases where the CO stretching frequency underwent a bathochromic (red) shift (*i.e.* it is lowered with respect to the CO gas phase frequency), usually not experimentally observed for CO adsorbed onto oxides with non-*d* cations, like the present case. Here, we elucidate in deep when and under which conditions this case may happen and concluded that this red shift may be related to peculiar surface sites occurring at the morphologically-complex Fo surfaces. The reasons for the red shift are linked to both the quadrupolar nature of the CO molecule and the role of dispersion interaction with surfaces of complex morphology. The present work, albeit speculative, suggest that, at variance with CO adsorption on simple oxides like MgO, the CO spectrum may exhibit features at lower frequencies than the reference gas frequency when CO is adsorbed on complex oxides, even in absence of transition metal ions.

I. INTRODUCTION

Carbon monoxide is a very common molecular probe in surface science since its vibrational stretching frequency strongly depends on the energetics and kind of adsorption.[1] When CO is adsorbed on exposed *d*-transitional metal cations, π-backdonation from *d* orbitals of the metal cation to the antibonding lowest unoccupied molecular orbital (LUMO) of the CO results in a weakening of the C–O bond and, as a consequence, in a lowering of the CO stretching frequency

with respect to the gas phase (*red* or *bathochromic shift*). On the contrary, σ-donation from the nonbonding highest occupied molecular orbital (HOMO) of CO produces a reinforcement of the C–O bond although of minor extent. For non-d/d^0 metals (as the case of Mg^{2+} in forsterite), where π-backdonation is prevented, the only possible interaction is the σ-donation (HOMO of CO → s/p orbital of the metal ion). Then, the CO stretching undergoes an *hypsochromic* or *blue shift* towards higher frequencies than the CO gas phase, as the C–O bond is reinforced.[2–6] It has been suggested that a large part of the interaction between CO and non-d/d^0 metals would be played by electrostatic:[7,8] the electric field exerted by the metal cation in its neighborhood where CO is located would produce a polarization of both σ- and π-CO bonding orbitals along the O→C direction, enhancing the strength of the CO bond.[9] Thus, the blue-shifted frequencies usually observed for CO adsorbed on pure non-d/d^0 ionic systems are the result of a charge-dipole interaction. However, it is worth underlining the fact that the vibrational shift does account for all specific interactions involving the CO molecule. While the dipolar nature of CO is usually emphasized in the literature, it exhibits a large quadrupole moment,[10–12] and a very small (in module) dipolar moment of 0.122 D,[13] as revealed by its electrostatic potential (ESP) map of Fig. 1.[13]

In a previous work, we anticipated how the quadrupolar nature of CO can affect its spectroscopic behavior when adsorbed on complex surfaces such as forsterite (Mg_2SiO_4, Fo) ones.[14] Within the present work, we expand upon the role of both quadrupolar and dispersion interactions in determining the vibrational properties of CO adsorbed on Fo surfaces, starting from our previous work.[14]

While our interest is focused on problems of astrochemical interest like CO on forsterite, the present results have a broader appeal, as they can be predictive of CO adsorbed on complex catalytically relevant materials or when CO is adsorbed on microporous materials in which the local adsorption sites are characterized by a high degree of morphological complexity.

A. Brief resume of our previous work

The aim of our previous work was to furnish a solid theoretical background for the adsorption process of CO – the second most abundant molecule in the interstellar medium (ISM) both in gas and solid phases[15,16] – on dust grains of the diffuse interstellar medium which are not covered in water ices.[17–22] Forsterite, the Mg-end member of the olivine solid solution, is one of the main components of silicon-based dust grains.[19–21] It exhibits isolated tetrahedral units (SiO$_4$) whose O atoms coordinate Mg ions in an octahedral fashion (MgO$_6$ units).[14,23]

To simulate CO adsorption on Fo surfaces, we defined 37 different initial geometries (spread among all surface models we used) where one or more CO molecules *per* unit cell are interacting with exposed Mg cations. All calculations have been performed with the CRYSTAL code,[24] at B3LYP-D2* level of theory[25–29] with a proper basis set which has been validated to give very good results in determining the structural features of forsterite ("Bruno's BS"),[14,23,30] with the addition of Ahlrichs VTZ + polarization functions (VTZ*) for the CO molecules.[31]

When cutting slabs from the bulk structure along selected [*hkl*] directions, we preserved the Fo silicate units (*i.e.* no covalent Si-O bonds have been cut) as well as the electrical neutrality,[32] leading to complex surfaces both from a morphological and electrostatic point of view, as shown in Fig. 1. Moreover, slabs models must have a sufficient thickness in order to ensure convergence in the associated surface energies (see Ref. 23 for the complete description of how Fo slabs have been generated).

For all 37 CO-(*hkl*) Fo cases, we run symmetry-free geometry optimizations allowing only the atomic positions to relax, while keeping slabs cell parameters fixed to the bulk values ("atomonly" optimizations). On the final optimized structures, we computed the CO stretching frequencies.

In 6 out of 37 cases, we observed CO frequency red-shifted, in clear contrast with what expected for CO interacting with non-*d* cations. Four out of these six are multi-loading cases where more than one CO molecule *per* cell were absorbed on different exposed Mg ions. There, red shifts can be explained by the repulsive lateral interactions among CO molecules in the same cell. However, the

remaining ones are mono-loading cases, free from lateral interactions. These two cases will be referred to in the following as "(110) 1C" and "(101) 1B". Numbers in parenthesis refer to the Miller indices of the Fo surface while 1C or 1B identifies the adsorption Mg ion sites labeled as C or B. To rationalize the red shifts, we noticed that, in both cases, an O atom of a nearby SiO$_4$ unit (hereafter labelled as "O$^-$") with an electric negative character, interacts with the "positive belt" of the CO quadrupole (see the CO ESP map in Fig. 1). We also suggested that the extents of the red shifts are related to the distance between the CO center of mass (CM) and the O$^-$ atom ($d_{\mathrm{CM-O^-}}$, in Å). To widen the basis of data related to this behavior by including the role of dispersion interactions and also to check carefully for numerical and method artifacts, we run, in the present work, further calculations.

It is worth mentioning that "(110) 1C" and "(101) 1B" are not the most stable cases for the (110) and (101) Fo surfaces, respectively. With respect to values reported in Table 3 of our previous work,[14] the CO adsorption enthalpies were equal to −20.9 and −38.1 kJ mol^{-1}, approximately half than the values for the most stable case (−40.7 and −63.2 kJ mol^{-1} for the (110) and (101) Fo surfaces, respectively). Thus, assuming a Boltzmann distribution, the relative occupation of these cases is essentially equal to zero, even at high temperatures and thus they may not contribute to the overall IR spectrum for CO adsorbed on Fo samples. However, we will prove here that the red shift effect is a robust and genuine one, and may be present (and observable) for more complex cases, like the amorphous silicates occurring in the ISM, or for complex oxides relevant in catalysis.

II. COMPUTATIONAL METHODS

The total DFT energy for the x species computed in the y geometry will be referred as $E_{\mathrm{Z}}(x//y)$, where the Z subscript denotes a periodic (Z = P, *i.e.* using periodic boundary conditions – PBC) or a molecular (Z = M, no PBC) calculation. Thus, the interaction energy *per* molecule of 2 CO with the Fo slabs (S) is given by Eq. (1)

$$\Delta E = \frac{E_\text{P}(S \cdot\cdot 2\text{CO}//S \cdot\cdot 2\text{CO}) - E_\text{P}(S//S) - 2E_\text{M}(\text{CO}//\text{CO})}{2} \tag{1}$$

where the factor 2 accounts for the fact that CO was adsorbed on both the top and bottom ends of the slab model. Eq. (1) does not account for the deformation of neither the slabs nor the CO molecules from their optimal geometries (δE_S and δE_CO, respectively), as well as the lateral interaction energy among CO molecules in different replicas of the unit cell (E_L). These quantities can be evaluated from Eq. (2)-(4)

$$\delta E_S = \frac{E_\text{P}(S//S \cdot\cdot 2\text{CO}) - E_\text{P}(S//S)}{2} \tag{2}$$

$$\delta E_\text{CO} = \frac{E_\text{M}(\text{CO}//S \cdot\cdot 2\text{CO}) - 2E_\text{M}(\text{CO}//\text{CO})}{2} \tag{3}$$

$$E_L = \frac{E_\text{P}(\text{CO}//S \cdot\cdot 2\text{CO}) - 2E_\text{M}(\text{CO}//S \cdot\cdot 2\text{CO})}{2} \tag{4}$$

When dealing with the CRYSTAL code, the Gaussian-based basis set originates the basis set superposition error (BSSE).[33,34] The main consequence of BSSE are two-folds: *i*) overestimation of interaction energies for complexes, usually corrected through the "counterpoise" (CP) method;[35] *ii*) a deformation of the potential energy surface, affecting the geometry optimization calculations. This second and more subtle effect is not corrected for in the present work. BSSE can be evaluated from Eq. (5) and (6):

$$\text{BSSE(S)} = \frac{E_\text{P}(S \cdot\cdot 2[\text{CO}]//S \cdot\cdot 2\text{CO}) - E_\text{P}(S//S \cdot\cdot 2\text{CO})}{2} \tag{5}$$

$$\text{BSSE(CO)} = \frac{E_\text{P}([S] \cdot\cdot 2\text{CO}//S \cdot\cdot 2\text{CO}) - E_\text{P}(S//S \cdot\cdot 2\text{CO})}{2} \tag{6}$$

where the square brackets denote "ghost functions".[35]

We computed the CP-corrected interaction energies ΔE^CP according to Eq. (7)

$$\Delta E^\text{CP} = \frac{\Delta E^* + \delta E_S + \delta E_\text{CO} + E_L - \text{BSSE}}{2} \tag{7}$$

where $\Delta E^* = \frac{1}{2}[E_\text{P}(S \cdot\cdot 2\text{CO}//S \cdot\cdot 2\text{CO}) - E_\text{P}(S//S \cdot\cdot 2\text{CO}) - E_\text{P}(\text{CO}//S \cdot\cdot 2\text{CO})]$ is the *deformation-free* interaction energy and BSSE is the sum of quantities in Eq. (5) and (6). If all the

energetic quantities are inclusive of the dispersion contributions, we label the CP-corrected interaction energies as ΔE^{CP} *disp*, otherwise as ΔE^{CP} *no disp*.

In order to test both the role of dispersive interactions (coupled with the electrostatic quadrupolar ones) and BSSE, we re-run optimizations and frequency calculations for the two cases at different levels of theory, namely B3LYP-D2* (the same approach used in our previous work), B3LYP-D3^{ABC},[36] B3LYP, PBE-D2 and PBE,[28,37] with the CRYSTAL code and PBE-D2 and PBE with the VASP code that – being based on plane waves basis sets – provides an important reference as results are not affected by the BSSE.[38–41] In CRYSTAL calculations, all other computational parameters (basis set, reciprocal-space sampling, DFT-integration, tolerances of Coulomb and exchange integrals, energetic and structural thresholds) were kept equal to the B3LYP-D2* ones of our original work, beside some further calculations with larger basis set and integration tolerances reported in the Supporting Information (SI) file available online.[14]

The quantities defined in Eq. (1)-(7) specifically refer to CRYSTAL calculations. For the VASP code, molecular calculations (E_M) have been simulated with a 20x20x20 Å unit cell, switching on the dipole correction (LDIPOL=.TRUE. and IDIPOL=4 in the code).[42]

In 2010, Tosoni and Sauer proposed to set the C_6 dispersion coefficient of the Mg^{2+} ion in MgO oxide to a value close to that of the corresponding Ne atom, in virtue of the negligible polarizability of a double charged Mg ion compared to the atomic value assumed by default in the Grimme's a posteriori correction[28] to the DFT energy.[43] They also led unchanged the C_6 for the oxygen ion, since it was shown to exist *a compensation between an increased polarizability and a decreased ionization potential* when passing from O to O^{2-}. Along the same line of thought, we run B3LYP-D2** (where the C_6 coefficient of Mg has been arbitrarily set equal to zero) calculations to comply with the Tosoni and Sauer recipe.

In VASP calculations, we used the PAW pseudopotential for core electrons and a plane-wave basis set for the valence electrons.[38,39] The plane-wave basis set kinetic cut-off was set equal to 500 eV.

The vacuum thickness of the slab was set to be 17 Å, large enough to decrease interactions among different replicas. The reciprocal-space sampling is analogous to the CRYSTAL case.

The energy threshold for the SCF iterative procedure in optimization and frequency calculations has been set equal to 10^{-5} and to 10^{-6} eV, respectively. In geometry optimizations, we set a 0.01 eV/Å threshold on the gradient.

On the optimized structures, we restricted the calculation of the harmonic IR frequencies in Γ-point[44,45] by diagonalizing the mass-weighted Hessian matrix.[44] Considering the very weak coupling between the CO stretching mode and other intermolecular modes, the complete phonon frequency calculations are restricted to CO molecules only, considered as fragments of the whole systems. This strategy has been validated by our research group in the past and has shown to be satisfactory.[46,47]

In order to partially recover errors associated to the adopted functional/basis set and anharmonicity, all the computed frequencies have been multiplied for proper scaling factors defined as the ratio between the CO gas phase experimental frequency (2143 cm^{-1}[;48]) and the computed stretching one. Thus, the vibrational scaled CO stretching shifts $\Delta\bar{v}^s$ are defined by Eq. (8):

$$\Delta\bar{v}^s = \bar{v}_{comp,ads} \cdot \frac{2143}{\bar{v}_{comp,free}} - 2143 \tag{8}$$

where $\bar{v}_{comp,ads}$ and $\bar{v}_{comp,free}$ are the computed stretching frequencies for adsorbed and free CO, respectively.

Finally, all VASP calculations have been performed with Gaussian smearing (ISMEAR = 0 in the code) with a small SIGMA value (0.01 eV). Please refer to SI file for further computational details.
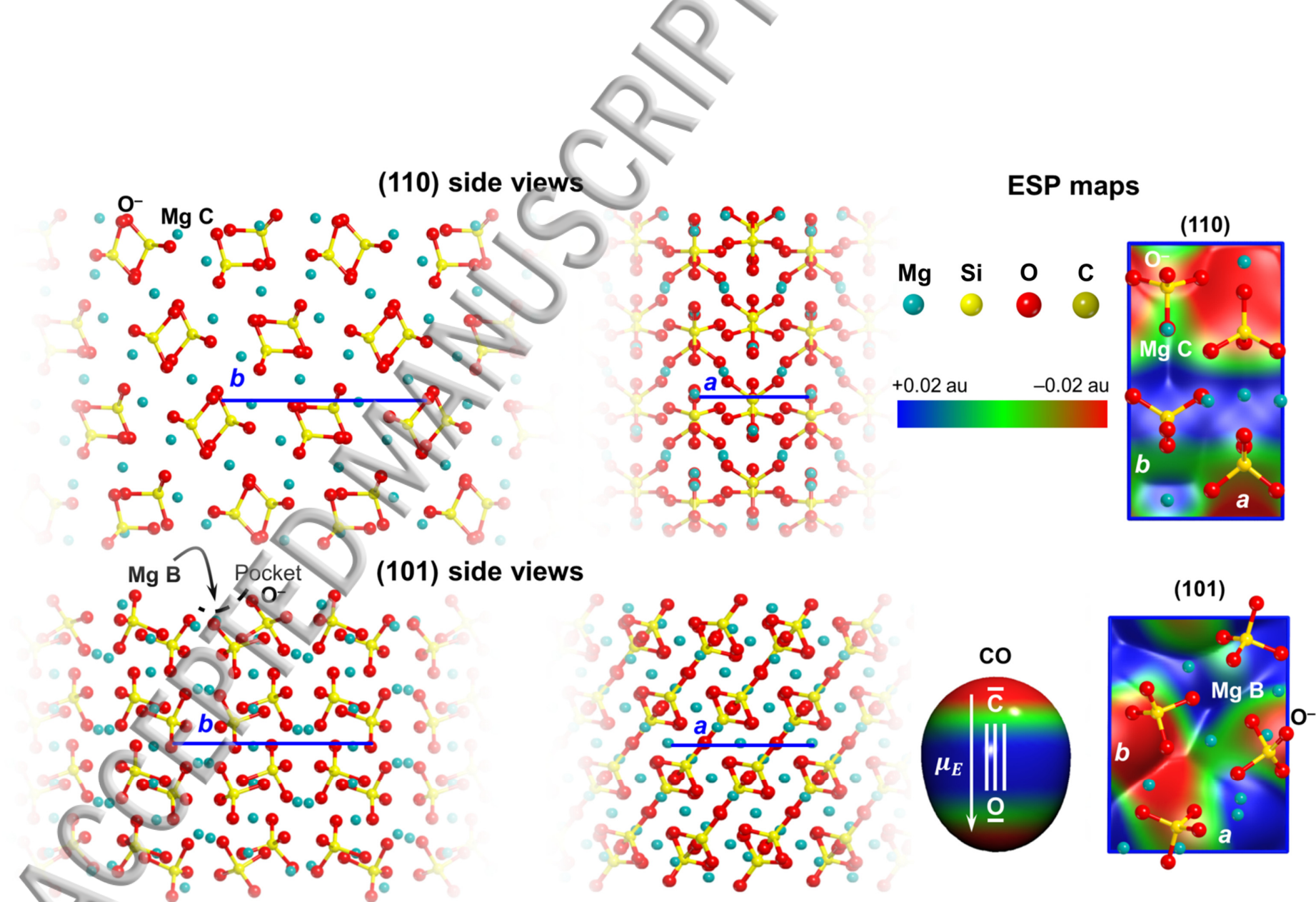
FIG. 1 Structural and electrostatic properties for the (110) and (101) forsterite surfaces and for the CO molecule. Left and center panels: side views along a and b lattice vectors. Right panel: electrostatic potential (ESP) maps superimposed to the electron density (ISO electron density value = 10^{-6} au). μ_E is the CO electric dipole moment: C and O atoms of CO represent the negative poles of the quadrupole, while the bond region is the "positive belt". Mg C, Mg B and O$^-$ atoms are also labeled for the sake of clarity. Lattice vectors in blue color.

III. RESULTS AND DISCUSSION

As already mentioned, in our previous work we run "atomonly" optimizations.[14] However, within this work, we observed a strong dependence of both the energetic and vibrational properties of CO adsorbed on Fo surfaces from the kind of geometry optimization. Thus, in order to remove all possible geometrical constraints, we decided to run full optimizations ("fullopt"), *i.e.* allowing both the atomic positions and the slabs cell parameters to fully relax within each selected Hamiltonian-dispersion method.

The energetic and vibrational properties for CO adsorbed on exposed non-d/d^0 cations of ionic surfaces mainly depends on electrostatic effects.[7,8] It is well known that several methods fail in the description of the correct orientation of the CO dipole ($C^{\delta-} \rightarrow O^{\delta+}$), and so of the quadrupole.[50] However, within both B3LYP/VTZ* and PBE/VTZ* methods (the dispersion correction does not significantly affect the distribution of charges), the orientations of both the CO dipole and quadrupole are correctly describe, as it is evident from the ESP map of CO in Fig. 1, even if the agreement between the computed and experimental values is not perfect (0.094 and 0.196 D for the module of the electric dipole and –1.37 and –1.34 D Å for the *zz* component of the quadrupole at B3LYP/VTZ* and PBE/VTZ*, respectively, to be compared with the experimental values of 0.122 D[13] and –2.63 D Å[11]).

All the computed energetic, vibrational and structural data for the two cases are resumed in Table I. In italics, we also report data from our previous work ("atomonly" optimizations at B3LYP-D2* level). As a first comment, when we allowed the slab parameters to fully relax at B3LYP-D2* level, the scaled vibrational shifts changes of 10 and 5 cm^{-1} for the "(110) 1C" and the "(101) 1B" cases, respectively, with the former becoming positive while the latter becoming more negative ("CRYSTAL B3LYP-D2*" rows in Table I). These very peculiar behaviors underline the strong dependence of the vibrational shifts of the kind of the adopted optimization procedure. We rationalize this dependence on the weak nature of the interaction, in which dispersion interaction drives the geometry, especially for the "(110) 1C case". Therefore, even small changes in the

surface geometry alter the potential energy surface to a sufficient extent to move the CO position and, consequently, its vibrational frequency.

For the sake of clarity, in Fig. 2 we report the side (panels I and II) and top (panels III) views of the final optimized geometries for the two cases obtained at B3LYP-D2* level. For all other functional/dispersion methods, the whole configurations are analogous. In panels IV, we provide a detailed zoom of the local atomistic environments surrounding the CO molecule. The three distances d_{C-Mg}, d_{CM-O^-} and d_{C-Mg} are also shown. They represent the carbon-magnesium distance, the distance between the CO center of mass and the surface O^- atom and the CO bond length, respectively.

TABLE I Resume of some computed energetic, spectroscopic and structural features for CO adsorbed on Mg C and B of the (110) and (101) forsterite surfaces, respectively. ΔE *no disp*: pure-DFT interaction energies. BSSE (%): BSSE contributions to the ΔE *no disp* values (percentages in parenthesis). ΔE^{CP} *no disp*: CP-corrected pure-DFT interaction energies. ΔE^{CP} *disp*: CP- and dispersion-corrected interaction energies. disp (%): dispersion contributions to the ΔE^{CP} *disp* values (percentages in parenthesis). δE_S: slabs-deformation energies. All these energetic quantities are in kJ mol^{-1} *per* adsorbed CO. $\Delta\bar{v}^s$: scaled vibrational CO stretching shifts (in cm^{-1}). d_{C-Mg}, d_{CM-O^-} and d_{C-O}: carbon-magnesium distances, CO centers of mass-O$^-$ distances and CO bond lengths (in Å). Reference values from our previous work ("atomonly" optimizations) in italics.[14]

Code	Functional-dispersion	ΔE *no disp*	BSSE (%)	ΔE^{CP} *no disp*	disp (%)	ΔE^{CP} *disp*	δE_S	$\Delta\bar{v}^s$	d_{C-Mg}	d_{CM-O^-}	d_{C-O}
					(110) 1C						
CRYSTAL	B3LYP-D2*	–31.8	–27.5 (86)	–4.4	–22.0 (83)	–26.4	15.2	–7	2.3298	2.6522	1.1268
CRYSTAL	B3LYP-D2*	–34.1	–25.3 (74)	–8.8	–13.9 (61)	–22.7	6.9	+3	2.3877	2.8010	1.1253
CRYSTAL	B3LYP-D2**	–34.7	–25.2 (73)	–9.4	–10.3 (52)	–19.7	3.6	+12	2.3778	2.9233	1.1244
CRYSTAL	B3LYP-D3^{ABC}	–32.5	–26.1 (80)	–6.5	–25.7 (80)	–32.2	8.0	–2	2.3657	2.7403	1.1261
CRYSTAL	B3LYP	–35.4	–24.5 (69)	–10.9	-	-	5.1	+15	2.4052	3.0318	1.1238
CRYSTAL	PBE-D2	–50.3	–31.6 (63)	–18.8	–16.1 (46)	–34.9	21.3	–59	2.2861	2.5385	1.1449
CRYSTAL	PBE	–51.6	–35.5 (61)	–20.1	-	-	19.1	–39	2.2891	2.5904	1.1422
VASP	PBE-D2	–19.1	-	–19.1	–15.1 (44)	–34.2	19.8	–25	2.3005	2.6303	1.1468
VASP	PBE	–22.9	-	–22.9		-	4.2	+13	2.3895	3.0998	1.1419
					(101) 1B						
CRYSTAL	*B3LYP-D2**	*–51.1*	*–26.2 (51)*	*–24.8*	*–18.7 (43)*	*–43.5*	*19.2*	*–21*	*2.2843*	*2.5731*	*1.1283*
CRYSTAL	B3LYP-D2*	–52.2	–26.2 (50)	–25.9	–15.0 (37)	–40.9	21.6	–26	2.2892	2.5609	1.1289
CRYSTAL	B3LYP-D2**	–50.4	–26.3 (52)	–24.1	–7.5 (24)	–31.6	24.6	–26	2.2931	2.5627	1.1288
CRYSTAL	B3LYP-D3^{ABC}	–50.3	–26.1 (52)	–23.9	–25.4 (52)	–49.3	23.3	–38	2.2781	2.5018	1.1305
CRYSTAL	B3LYP	–45.9	–23.1 (50)	–22.8	-	-	6.6	+28	2.3359	2.9541	1.1221
CRYSTAL	PBE-D2	–70.5	–31.6 (43)	–40.5	–13.9 (26)	–54.4	27.2	–90	2.2494	2.3840	1.1499
CRYSTAL	PBE	–70.0	–31.5 (43)	–39.8	-	-	31.9	–97	2.2578	2.3681	1.1508
VASP	PBE-D2	–52.4	-	–52.4	–11.9 (19)	–64.3	18.6	–71	2.2732	2.4225	1.1533
VASP	PBE	–50.0	-	–50.5	-	-	22.3	–76	2.2825	2.4026	1.1541

A. Energetic analysis

The total DFT-D CP-corrected interaction energies (ΔE^{CP} *disp* in Table I) are highly sensitive to the level of adopted functional. Leaving aside the dispersion correction, B3LYP values are almost half of the corresponding PBE ones. This can be rationalized by the well-known evidence that Becke's exchange is over-repulsive compared to the Perdew's one, the latter showing spurious attraction mimicking in some way the dispersion contribution even for noble gas dimers (the interested reader can look at Ref. 51). In turn, the more attractive PBE functional brings CO closer to the Fo surface (see d_{C-Mg} and d_{CM-O}- values in Table I, 10th and 11th columns) with consequences also on the CO stretching frequency shift, which moves from hypsochromic (B3LYP) to bathochromic (PBE) values (see section III.B).

Dispersive contribution to the interaction energy is sizeable (data of Table I), accounting for up to 80% of the total ΔE^{CP} *disp* interaction energies ("disp (%)" column of Table I). Therefore, the choice of a specific dispersion correction recipe may be crucial when dealing with CO adsorption on complex surfaces as the Fo ones, and even on simpler systems, like the MgO surfaces.[52] The best correction for systems containing highly charged metal ions, like in the present case, is the D2** or similar ones. The B3LYP-D3[ABC] overestimates the energetic of adsorption when compared with other B3LYP "fullopt" methods. Indeed, D3[ABC] contributions are larger (in percentage) than other dispersion methods (6th column of Table I).

The computed interactions energies of B3LYP and PBE (both with CRYSTAL and VASP) are very similar to the ΔE^{CP} *no disp* ones (*i.e.* the total DFT interaction energies purified by the dispersion contributions) computed at B3LYP-D2*/D2** and PBE-D2 levels, with a discrepancy of $\sim \pm 2.0$ kJ mol^{-1}. This means the large variability that we observed in the spectroscopic and structural properties of CO adsorption (see Section 3.2) is mainly due to the different dispersive contribution accounted for by the various kinds of post-DFT corrections.
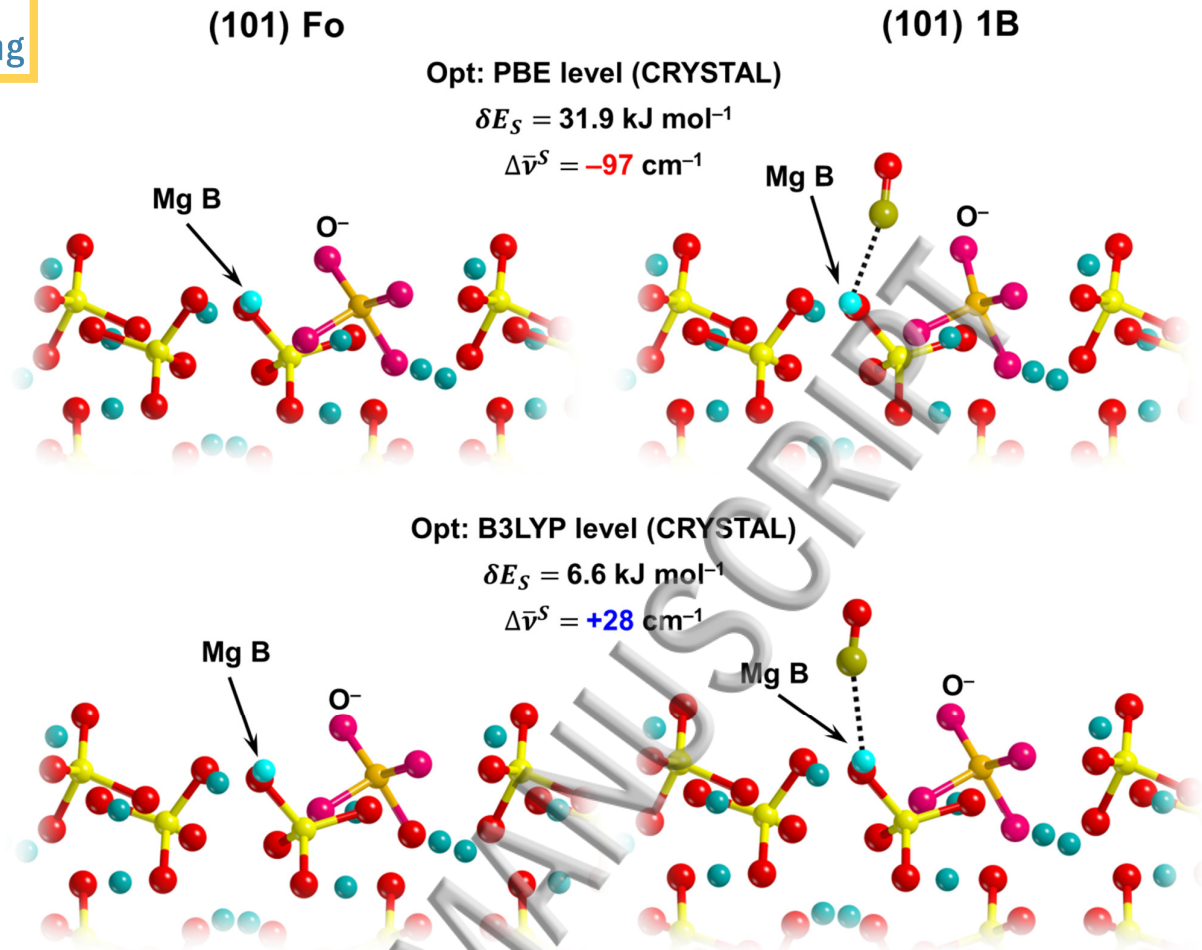
As the dispersion correction is, in general, attractive, it brings CO closer to the Fo surface with a further increase of the BSSE. Therefore, it is expected that the synergy between BSSE and

dispersion contribution affects the structural and, consequently, the vibrational features of CO adsorbed on Fo surfaces. This is particularly true for the "(110) 1C" case. The final optimized geometries assumed by the CO molecule in the two cases show, for the "(110) 1C", a CO lying almost parallel to the Fo surface, while for the "(101) 1B" case CO is almost perpendicular to the surface (see Fig. 2). As a consequence, the former is more sensitive to lateral (quadrupolar) and non-specific (dispersive) interactions than the latter.

Slab-deformation energies (δE_S) show a large variability as they spread in a wide ~6-32 kJ mol^{-1} range of values (8th column of Table I). Values greater than 18-20 kJ mol^{-1} can be associated with large movements of the SiO$_4$ units from their optimal positions. As an example, in Fig. 3 we reported the final optimized geometries for "(101) 1B" case computed at PBE (top panels) and B3LYP (bottom panels) levels with the CRYSTAL code (highest and lowest δE_S values among the "(101) 1B" cases, respectively). At PBE level, the Mg cation and the SiO$_4$ unit involved in the interaction with the CO (highlighted with a different color code) move significantly due to CO adsorption, while at B3LYP level this does not occur. As a general comment, high slab-deformation energies are related with strong red-shifts, although a strict correlation does not exist.
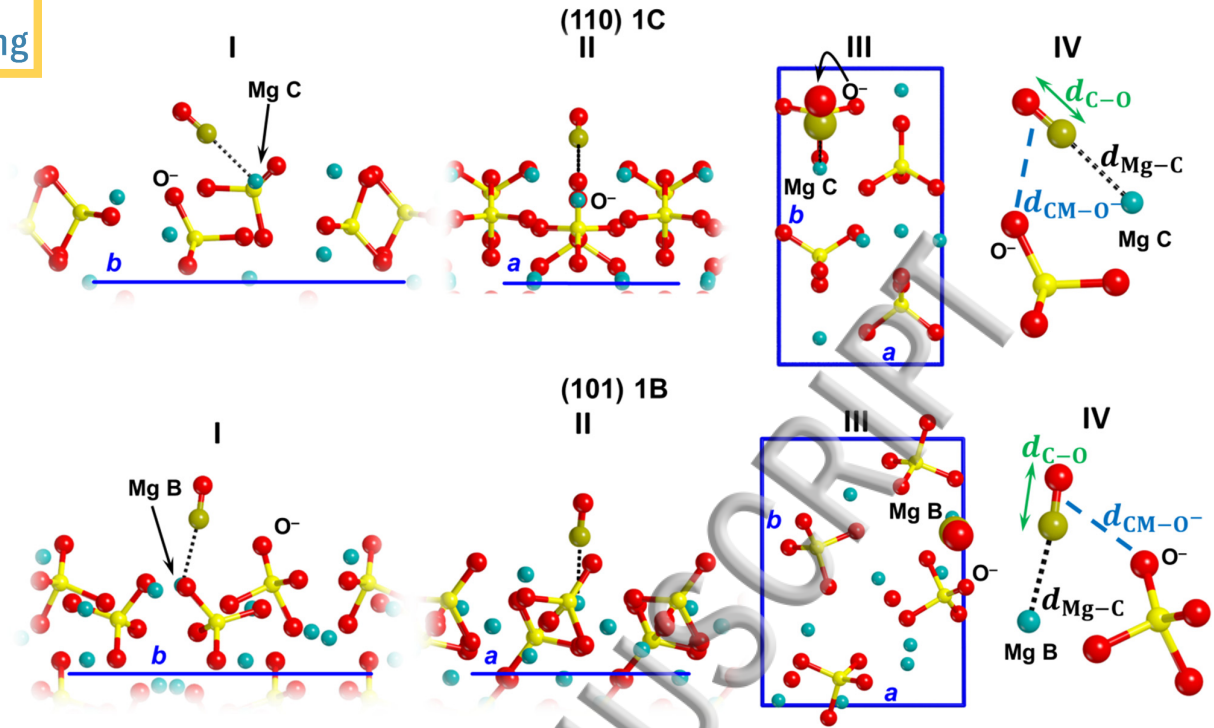
FIG. 2 Final optimized geometries for the "(110) 1C" (top) and "(101) 1B" (bottom) cases computed at B3LYP-D2* level. The structural features for all other cases are analogous. I and II: details of the side views along a and b lattice vectors. III: top views (C and O atoms of the CO molecules as van der Waals spheres). IV: Zoomed views of the local atomic environments surrounding the CO molecule; the three distances reported in Table 1 are also highlighted.

(101) Fo   **(101) 1B**

Opt: PBE level (CRYSTAL)

$$\delta E_S = 31.9 \text{ kJ mol}^{-1}$$

$$\Delta \bar{\nu}^S = -97 \text{ cm}^{-1}$$

Opt: B3LYP level (CRYSTAL)

$$\delta E_S = 6.6 \text{ kJ mol}^{-1}$$

$$\Delta \bar{\nu}^S = +28 \text{ cm}^{-1}$$

FIG. 3 Comparison between the final optimized geometries of the pure (101) Fo slab (left) and the "(101) 1B" case (right) computed at PBE (top) and B3LYP (bottom) level of theory (detailed, zoomed views are only reported). At PBE level, there is a large structural rearrangement of both Mg B and the silicate unit carrying the O⁻ atom, while at B3LYP level this does not occur. For the sake of clarity, we highlighted these atoms with a different color code (Mg B in cyan, Si and O atoms of the SiO₄ units in ochre and magenta, respectively).

B. Vibrational shifts

As already stated, CO red-shits are not usually observed from experiments. One possible reason for their appearance in simulations may be related to "computational artifact" due to BSSE. However, present calculation with the VASP code envisaging BSSE-free plane wave basis set, carried out at PBE and PBE-D2 levels (Table I, 9th column), still provide red shifts, whose absolute values depend on both the case analyzed and the presence of dispersion correction. We can therefore exclude the BSSE affecting the CRYSTAL calculations as the cause of the red-shift.

For the "(101) 1B" case, which is characterized by a stronger interaction energy compared to the "(110) 1C" one, and where BSSE and dispersion accounts for a minor part of the interaction, results are less sensitive to the level of theory and there is strong evidence of a red-shifted CO frequency. For instance, full B3LYP-D2* geometrical optimizations only slightly affect the vibrational shifts compared to the "atomonly" case (from -21 to -26 cm^{-1}). With the exclusion of B3LYP results (no dispersion), the CO frequency is always red-shifted, albeit with definite dependence of the adopted method. Changing the DFT functional from B3LYP to PBE (CRYSTAL code) has a dramatic effect on the vibrational shift that lowers by several tens of cm^{-1}, becoming largely negative (-90 and -97 at PBE-D2 and PBE level, respectively). Consequently, $d_{\mathrm{C-Mg}}$ and $d_{\mathrm{CM-O^-}}$ distances decrease.

The vibrational shift for "(110) 1C" case is highly sensitive to the adopted level of theory. Indeed, the original "atomonly" optimization at B3LYP-D2* level (row in italics in Table I) shows a -7 cm^{-1} value for the shift, while, after the removal of any geometrical constraint, the shift becomes slightly positive ($+3$ cm^{-1}). At B3LYP-D2** or at dispersion-free B3LYP levels, the vibrational shift further increases ($+12$ and $+15$ cm^{-1}, respectively). The addition of the D3^{ABC} correction term results in a lowering of the vibrational shift that went back to a slightly negative (-2 cm^{-1}) value. This lowering from $+12/+15$ to -2 cm^{-1} is probably the result of the over-correction due to the D3^{ABC} term that brings CO closer to the Fo surface, (and thus to the Mg ion and the O$^-$ atom, see

16

d_{C-Mg} and d_{CM-O^-} values of Table I, 10th and 11th columns), in agreement with the behavior for the "(101) 1B" case.

The CRYSTAL/VASP comparison at PBE(-D2) level apparently show some inconsistencies. For the "(101) 1B" case, CRYSTAL and VASP data are in good accordance, since both spectroscopic and structural data match well. For the weakest "(110 1C)" case, the removal of D2 contribution in VASP optimizations strongly affects the vibrational shift that switches from a negative (-25 cm^{-1}) to a positive ($+13$ cm^{-1}) value. In CRYSTAL optimizations, this does not occur, even if the vibrational shift increases from -59 to -39 cm^{-1}. This discrepancy can be rationalized by invoking again the role of BSSE, absent in VASP calculations, which is more important for this weakly bounded case. Indeed, in absence of other (strongly) bounding energetic factors as BSSE and dispersion, "(110) 1C" case actually does not show a red-shifted CO stretching frequency, as originally reported in our previous work.[14] Thus, this discrepancy for this specific case is the symptom that a spurious attraction due to BSSE in CRYSTAL PBE(-D2) optimization is causing the CO to stay too close to the site with a consequent red-shifted frequency. On the contrary, data for "(101) 1B" suggest that a physical electrostatic interaction causing the red shift is actually occurring for such case, even when the over-repulsive Becke's exchange is included. To shed some lights on this point, we run further calculations with an enhanced QZP* basis set at PBE, in order to decrease the role of BSSE (see the SI file). Data from these higher-level computations strengthen our conclusion about the role of BSSE in the two tested cases.

It is well known that the energetic and vibrational properties of CO adsorbed on exposed Ca^{2+}, Na$^+$, Zn^{2+}, Ag$^+$, and Cu$^+$ cations of exchanged zeolites exhibit a linear correlation, as a consequence of the charge-dipole interaction.[53] However, for Fo surfaces – which are more complex both from an electrostatic and morphological point of view than exchanged zeolites – we did not observe such linear correlations because of the role played by quadrupolar interactions. Nevertheless, a very good linear correlation between the vibrational shifts and the C–O bond lengths (d_{C-O}) resulted, as

17

shown in the top-left panel of Fig. 4 for B3LYP-based calculations (irrespective of the kind of dispersion scheme adopted). In the top-right panel, CRYSTAL and VASP results are contrasted for the same quantities at PBE level. As expected, the correlation graphs are method-dependent, which is in line with the different basis set and methodological differences (BSSE, numerical accuracy, etc.). For instance, the bond length and the absolute stretching frequency of gas phase CO are: PBE CRYSTAL: 1.1368 Å and 2118 cm^{-1}; PBE VASP: 1.1432 Å and 2126 cm^{-1}. Interestingly, while the different intercepts are linked to these systematic differences, the slopes are very close, revealing that both approaches give a similar response of CO to the external field.

In our previous work, we hypothesized that the CO red shifts may correlate with the distance between the CO center of mass and the neighbor O$^-$ atoms (d_{CM-O^-}).[14] The present simulations seem to confirm our hypothesis. With reference to the bottom panels of Fig. 4, we revealed the existence of two distinct linear correlations between d_{CM-O^-} values and the red shifts for the two tested cases, regardless the adopted functional-dispersion/basis set method. These linear correlations do not occur if we also include blue shift values (blue circles) suggesting the existence of a "cut-off distance" for which the quadrupolar interaction involving the positive belt of the CO quadrupole vanishes. These cut-off distances are 2.73 and 2.62 Å (extrapolation to $\Delta\bar{\nu}^s = 0$ cm^{-1} of the two correlation lines) for the "(110) 1C" and "(101) 1B" case, respectively. Actually, for all blue-shifted cases, d_{CM-O^-} values are larger than the predicted cut-offs.

In order to strengthen this point, we run further calculations on a very simple system made by one CO molecule interacting with a single MgO unit. This simplified model "cleans up" all other interactions involving the CO molecule that occur in the Fo slabs. Data collected for these CO+MgO system (see SI for full account) confirm the robustness of the described linear correlations.
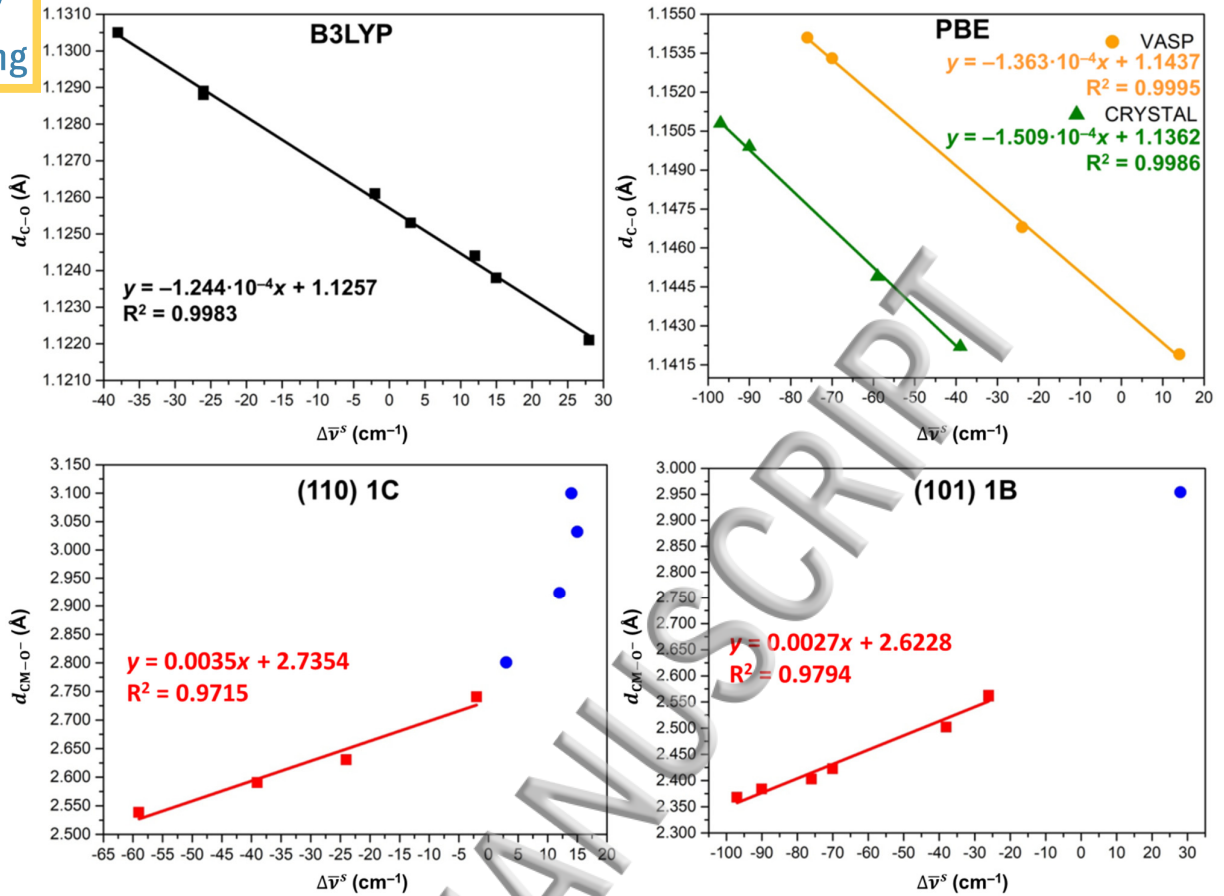
FIG. 4 Linear correlations (only "fullopt" data). Top panels: C–O bond lengths (d_{C-O}) *vs* scaled vibrational shifts ($\Delta\bar{\nu}^s$) for the B3LYP (left) and PBE (right) functionals. Bottom panels: distances between the CO center of mass and the O⁻ atoms (d_{CM-O^-}) *vs* $\Delta\bar{\nu}^s$ for the "(110) 1C" (left) and "(101) 1B" cases. Only negative shifts (red squares) correlate with d_{CM-O^-} values.

IV. CONCLUSIONS

In our previous work, we reported red-shifts (with respect the gas phase value) of the carbon monoxide IR stretching frequency when adsorbed on exposed Mg ions (non-*d* cations) of the forsterite (Mg_2SiO_4, Fo) surfaces, even for very low CO-coverage (one CO molecule *per* unit cell).[14] This is in contrast with the case of CO adsorbed on simple flat ionic surfaces such as the (001) MgO or cation-exchanged zeolites ones,[54,55] where the calculations predict blue shifted frequency, in agreement with the experiments.[7,8] However, crystalline Fo surfaces are in general not flat: the presence of different exposed negatively-charged bulky SiO_4 units, together with the attractive dispersive component of the interaction energy, highlight the role of the interaction between Fo surface and the CO quadrupole moment. This rather complex interplay between dispersion and electrostatic leads to a CO frequency red-shift, a result that, up to now, has no counterpart in experiments and has never been reported even in simulation studies. Our analysis revealed that the extent of the red shift can be related with the distance between the CO center of mass and the closest negative O atoms of a nearby SiO_4 surface units and is related to the quadrupolar nature of CO. We adopted B3LYP level with different versions of Grimme's correction for dispersion with the CRYSTAL code for two representative cases characterized by different strength of the CO interaction energy. We also compared PBE(-D2) results with the CRYSTAL and VASP codes to elucidate the role of BSSE present when a Gaussian basis set is adopted. The comparison of all computed data confirms that, for some specific configurations, CO frequency is red-shifted resulting from physical interactions with peculiar sites occurring at the Fo surfaces, and not from artifacts due to the BSSE. Why CO bathochromic shifts have never been observed experimentally remains an open question. Reasons may be related to the difficulty of stabilizing case like the ones analyzed in the present work, compared to the most stable situations which are closer to the standard model of CO adsorption. Indeed, if these cases have very small populations, the associated intensity will not be easily revealed in a spectral region which is always attributed to the CO liquid phase. However, we believe this work may provide indication that the simple

20

charge/dipole moment adopted since long ago to explain the CO interacting with cations at the ionic surfaces may not be the exclusive mechanism, especially when CO is used to probe the surface of more complex materials.

AUTHORS INFORMATION

Corresponding author

Piero Ugliengo, piero.ugliengo@unito.it, telephone: +39 011 670 4596

ORCID

Lorenzo Zamirri: 0000-0003-0219-6150

Stefano Pantaleone: 0000-0002-2457-1065

Piero Ugliengo: 0000-0001-8886-9832

SUPPORTING INFORMATION FILE

In the Supporting Information file available online we provide further computational details (CRYSTAL single point, geometry optimizations and frequency calculations, basis sets, reciprocal-lattice sampling, convergence thresholds, DFT-integration and smearing of the Fermi level in VASP), results concerning with the QZP* basis set and the spectroscopic and structural data for the CO+MgO benchmark system.

REFERENCES

[1] G. Pacchioni and P.S. Bagus, in *Clust. Model. Surf. Bulk Phenom.*, edited by G. Pacchioni, P.S. Bagus, and F. Parmigiani, NATO ASI S (Springer, Boston, MA, USA, 1992), pp. 304–320.

[2] J. Pilme, B. Silvi, and M.E. Alikhanim, J. Phys. Chem. A **107**, 4506 (2003).

[3] D. Tiana, E. Francisco, M.A. Blanco, P. Macchi, A. Sironi, and A. Martín Pendás, J. Chem. Theory Comput. 6, 1064 (2010).

[4] G. Bistoni, S. Rampino, N. Scafuri, G. Ciancaleoni, D. Zuccaccia, L. Belpassi, and F. Tarantelli, Chem. Sci. **7**, 1174 (2016).

[5] G. Blyholder, J. Phys. Chem. **68**, 2772 (1964).

[6] S. Sicolo and G. Pacchioni, Surf. Sci. **602**, 2801 (2008).

[7] A.S. Goldman and K. Krogh-Jespersen, J. Am. Chem. Soc. **118**, 12159 (1996).

[8] A.J. Lupinetti, S. Fau, G. Frenking, and S.H. Strauss, J. Phys. Chem. A **101**, 9551 (1997).

[9] A.M. Ferrari, P. Ugliengo, and E. Garrone, J. Chem. Phys. **105**, 4129 (1996).

[10] C. Graham, D.A. Imrie, and R.E. Raab, Mol. Phys. **93**, 49 (1998).

[11] N. Chetty and V.W. Couling, J. Chem. Phys. **134**, 164307(1 (2011).

[12] G. Pacchioni, G. Cogliandro, and P.S. Bagus, Int. J. Quantum Chem. **42**, 1115 (1992).

[13] J. Muenter, J. Mol. Spectrosc. **55**, 490 (1975).

[14] L. Zamirri, M. Corno, A. Rimola, and P. Ugliengo, ACS Earth Sp. Chem. **1**, 384 (2017).

[15] P. Ehrenfreund and S.B. Charnley, Annu. Rev. Astron. Astrophys. **38**, 427 (2000).

[16] L.J. Allamandola, M.P. Bernstein, S.A. Sandford, and R.L. Walker, Space Sci. Rev. **90**, 219 (1999).

[17] A. Li and B.T. Draine, Astrophys. J. **550**, L213 (2001).

[18] F.J. Molster, I. Yamamura, L.B.F.M. Waters, A.G.G.M. Tielens, T. de Graauw, T. de Jong, A. de Koter, K. Malfait, M.E. van den Ancker, H. van Winckel, R.H.M. Voors, and C. Waelkens, Nature **401**, 563 (1999).

[19] T. Henning, in *Solid State Astrochem.*, edited by V. Pirronello, J. Krelowski, and G. Manicò (Proceedings of the NATO Advanced Study Institute on Solid State Astrochemistry, 2000), pp. 85–103.

[20] T. Henning, Annu. Rev. Astron. Astrophys. **48**, 21 (2010).

[21] F.J. Molster and C. Kemper, Space Sci. Rev. **119**, 3 (2005).

[22] G.J. Melnick and E.A. Bergin, Adv. Sp. Res. **36**, 1027 (2005).

[23] M. Bruno, F.R. Massaro, M. Prencipe, R. Demichelis, M. De La Pierre, and F. Nestola, J. Phys. Chem. C **118**, 2498 (2014).

[24] R. Dovesi, V.R. Saunders, C. Roetti, R. Orlando, F. Pascale, B. Civalleri, K. Doll, N.M. Harrison, I.J. Bush, P. D'Arco, M. Llunel, M. Causà, Y. Noël, L. Maschio, A. Erba, M. Rérat, and S. Casassa, (2018).

[25] A.D. Becke, Phys. Rev. A **38**, 3098 (1988).

[26] A.D. Becke, J. Chem. Phys. **98**, 1372 (1993).

[27] C. Lee, C. Hill, and N. Carolina, Phys. Rev. B **37**, 785 (1988).

[28] S. Grimme, J. Comput. Chem. **27**, 1787 (2006).

[29] B. Civalleri, C.M. Zicovich-Wilson, L. Valenzano, and P. Ugliengo, CrystEngComm **10**, 405 (2008).

[30] R. Demichelis, M. Bruno, F.R. Massaro, M. Prencipe, M. de la Pierre, and F. Nestola, J. Comput. Chem. **36**, 1439 (2015).

[31] A. Schäfer, H. Horn, and R. Ahlrichs, J. Chem. Phys. **97**, 2571 (1992).

[32] G.W. Watson and P.M. Oliver, Phys. Chem. Miner. **25**, 70 (1997).

[33] H.B. Jansen and P. Ros, Chem. Phys. Lett. **3**, 140 (1969).

[34] B. Liu and A.D. Mclean, J. Chem. Phys. **59**, 4557 (1973).

[35] S.F. Boys and F. Bernardi, Mol. Phys. **19**, 553 (1970).

[36] S. Grimme, J. Antony, S. Ehrlich, and H. Krieg, J. Chem. Phys. **132**, 154104(1 (2010).

[37] J.P. Perdew, K. Burke, and M. Ernzerhof, Phys. Rev. Lett. **77**, 3865 (1996).

[38] D. Joubert, Phys. Rev. B **59**, 1758 (2014).

[39] P.E. Blöchl, Phys. Rev. B **50**, 17953 (1994).

[40] G. Kresse and J. Furthmüller, Phys. Rev. B **54**, 11169 (1996).

[41] G. Kresse and J. Furthmüller, Comput. Mater. Sci. **6**, 15 (1996).

[42] G. Kresse, M. Marsman, and J. Furthmüller, https://www.vasp.at/index.php/Ddocumentation.

[43] S. Tosoni and J. Sauer, Phys. Chem. Chem. Phys. **12**, 14330 (2010).

[44] F. Pascale, C.M. Zicovich-Wilson, F. López Gejo, B. Civalleri, R. Orlando, and R. Dovesi, J. Comput. Chem. **25**, 888−897 (2004).

[45] C.M. Zicovich-Wilson, F. Pascale, C. Roetti, V.R. Saunders, R. Orlando, and R. Dovesi, J. Comput. Chem. **25**, 1873−1881 (2004).

[46] S. Tosoni, F. Pascale, P. Ugliengo, R. Orlando, V.R. Saunders, and R. Dovesi, Mol. Phys. **103**, 2549−2558 (2005).

[47] L. Zamirri, S. Casassa, A. Rimola, M. Segado-Centellas, C. Ceccarelli, and P. Ugliengo, Mon. Not. R. Astron. Soc. **480**, 1427 (2018).

[48] N. Mina-Camilde, C.I. Manzanares, and J.F. Caballero, J. Chem. Educ. **73**, 804 (1996).

[49] M. Methfessel and A.T. Paxton, Phys. Rev. B **40**, 3616 (1989).

[50] G.E. Scuseria, M.D. Miller, F. Jensen, and J. Geertsen, J. Chem. Phys. **94**, 6660 (1991).

[51] X. Wu, M.C. Vargas, S. Nayak, V. Lotrich, and G. Scoles, J. Chem. Phys. **115**, 8748 (2001).

[52] A. Damin, R. Dovesi, A. Zecchina, and P. Ugliengo, Surf. Sci. **479**, 255 (2001).

[53] V. Bolis, G. Magnacca, and C. Morterra, Res. Chem. Intermed. **25**, 25 (1999).

[54] B. Civalleri, L. Maschio, P. Ugliengo, and C.M. Zicovich-Wilson, Phys. Chem. Chem. Phys. **12**, 6382 (2010).

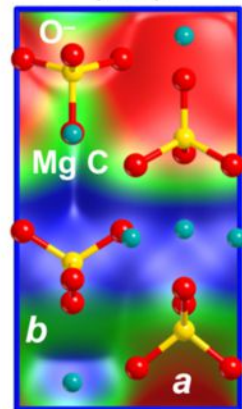[55] V. Bolis, A. Barbaglia, S. Bordiga, C. Lamberti, and A. Zecchina, J. Phys. Chem. B **108**, 9970 (2004).
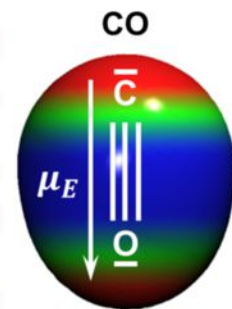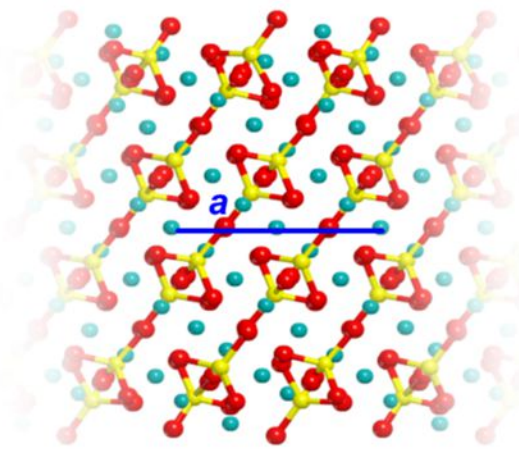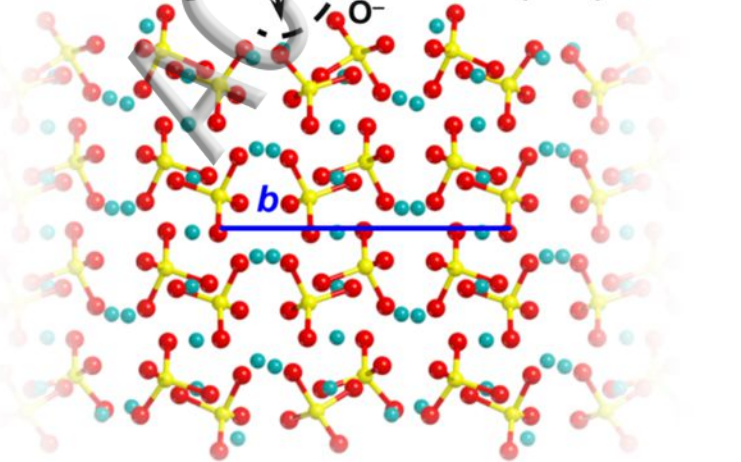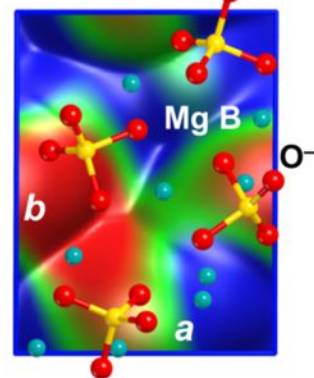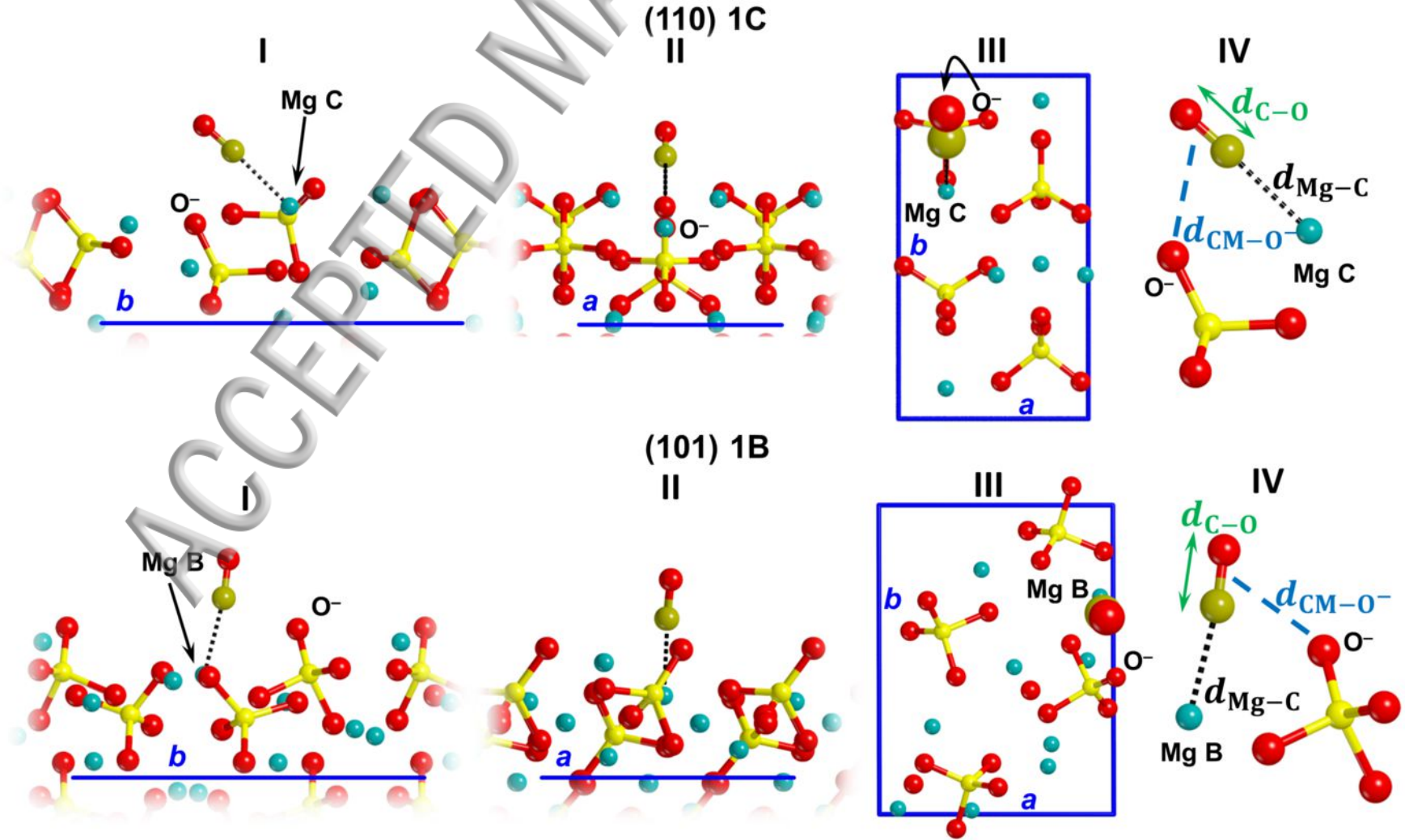
(110) side views   ESP maps
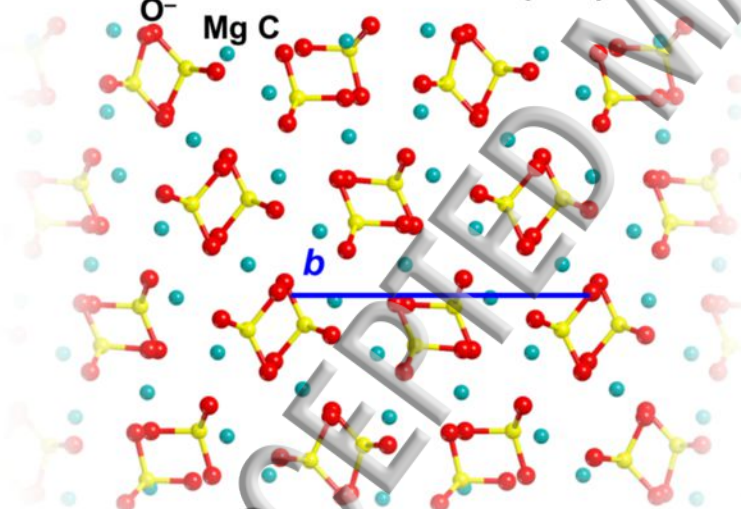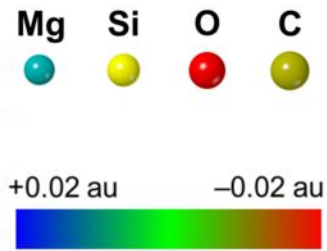
(101) side views

(101) Fo   **(101) 1B**

Opt: PBE level (CRYSTAL)

$\delta E_S = 31.9$ kJ mol^{-1}

$\Delta \bar{\nu}^S = -97$ cm^{-1}

Mg B   O$^-$ Mg B   O$^-$

Opt: B3LYP level (CRYSTAL)

$\delta E_S = 6.6$ kJ mol^{-1}

$\Delta \bar{\nu}^S = +28$ cm^{-1}

Mg B   O$^-$ Mg B   O$^-$

B3LYP

$y = -1.244 \cdot 10^{-4}x + 1.1257$
$R^2 = 0.9983$

PBE

● VASP
$y = -1.363 \cdot 10^{-4}x + 1.1437$
$R^2 = 0.9995$
▲ CRYSTAL
$y = -1.509 \cdot 10^{-4}x + 1.1362$
$R^2 = 0.9986$

(110) 1C

$y = 0.0035x + 2.7354$
$R^2 = 0.9715$

(101) 1B

$y = 0.0027x + 2.6228$
$R^2 = 0.9794$